Journal of Structural Biology 199 (2017) 68–75

Contents lists available at ScienceDirect

Journal of Structural Biology

journal homepage: www.elsevier.com/locate/yjsbi

Substrate-analog binding and electrostatic surfaces of human manganese superoxide dismutase

Jahaun Azadmanesh [a,b], Scott R. Trickel [a], Gloria E.O. Borgstahl [a,b,*]

[a] The Eppley Institute for Research in Cancer and Allied Diseases, 987696 Nebraska Medical Center, Omaha, NE 68198-7696, USA
[b] Department of Biochemistry and Molecular Biology, 985870 Nebraska Medical Center, Omaha, NE 68198-5870, USA

ARTICLE INFO

Article history:
Received 6 December 2016
Received in revised form 10 April 2017
Accepted 27 April 2017
Available online 29 April 2017

Keywords:
Superoxide dismutase enzyme
X-ray crystallography
Electrostatic guidance
Reactive oxygen species
Mitochondria

ABSTRACT

Superoxide dismutases (SODs) are enzymes that play a key role in protecting cells from toxic oxygen metabolites by disproportionation of two molecules of superoxide into molecular oxygen and hydrogen peroxide via cyclic reduction and oxidation at the active site metal. The azide anion is a potent competitive inhibitor that binds directly to the metal and is used as a substrate analog to superoxide in studies of SOD. The crystal structure of human MnSOD-azide complex was solved and shows the putative binding position of superoxide, providing a model for binding to the active site. Azide is bound end-on at the sixth coordinate position of the manganese ion. Tetrameric electrostatic surfaces were calculated incorporating accurate partial charges for the active site in three states, including a state with superoxide coordinated to the metal using the position of azide as a model. These show facilitation of the anionic ligand to the active site pit via a 'valley' of positively-charged surface patches. Surrounding ridges of negative charge help guide the superoxide anion. Within the active site pit, Arg173 and Glu162 further guide and align superoxide for efficient catalysis. Superoxide coordination at the sixth position causes the electrostatic surface of the active site pit to become nearly neutral. A model for electrostatic-mediated diffusion, and efficient binding of superoxide for catalysis is presented.

1. Introduction

Superoxide dismutases (SODs) are essential antioxidant enzymes that protect cells from reactive oxygen species and promote health and longevity. In eukaryotes, MnSOD is found in the mitochondrial matrix and remediates superoxide generated by the electron transport chain (McCord, 2002). Mice with MnSOD knocked out die within the first 10 days of life and overexpression of MnSOD in fruit flies results in increased life span (Li et al., 1995; Sun et al., 2002). Mutations in human MnSOD are linked to neurological disorders, cancer, and late-onset diseases (Kim, 2010; Perry et al., 2007). In each enzymatic cycle, two superoxide ions are converted into molecular oxygen and hydrogen peroxide via cyclic reduction and oxidation at the active site metal (Holm et al., 1996). The following is an overview of the MnSOD enzymatic reaction.

$$Mn^{3+} + O_2^{\cdot-} \rightarrow Mn^{2+} + O_2$$
$$Mn^{2+} + O_2^{\cdot-} + 2H^+ \rightarrow Mn^{3+} + H_2O_2$$

Human MnSOD functions as a tetramer and is rate-limited only by diffusion of its substrates and products (Bannister and Bannister, 1987). The active site manganese ion is coordinated by His26, His74, Asp159, His163, and a single oxygen, typically thought to be a water or hydroxide ion (Fig. 1). These ligands are referred to as the "inner-sphere" residues. "Outer-sphere" residues surround the inner-sphere and include His30, Tyr34, Phe77, Trp78, Trp123, Gln143, Trp161 and, from across the dimer interface, Glu162. The substrate approaches the active site along a trajectory between His30 and Tyr34 and binds in the position opposite Asp159. Hydrophobic residues Phe77, Trp78, Trp123 and Trp161 form a hydrophobic cage around the base of the active site, trapping ligands and solvent to facilitate catalysis by the manganese ion (Hearn et al., 2001). His30, Tyr34 and Gln143 are thought to provide a hydrogen-bond network for proton donation to the active site in addition to orienting solvent for proton transfer (Edwards et al., 2001b; Leveque et al., 2000; Perry et al., 2009;

Abbreviation: SOD, superoxide dismutase.

* Corresponding author at: The Eppley Institute for Research in Cancer and Allied Diseases, 987696 Nebraska Medical Center, Omaha, NE 68198-7696, USA.
E-mail address: gborgstahl@unmc.edu (G.E.O. Borgstahl).

http://dx.doi.org/10.1016/j.jsb.2017.04.011
1047-8477/

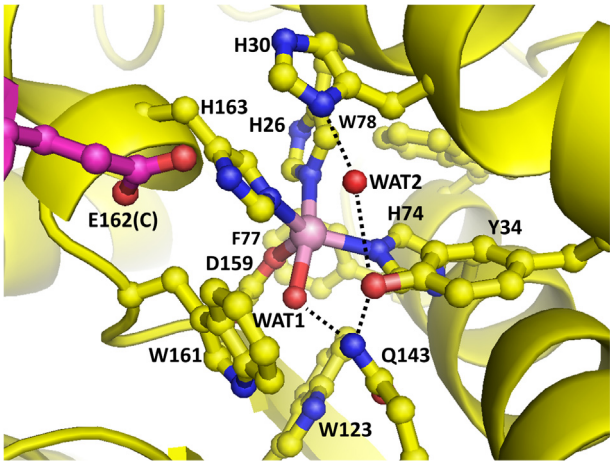

Fig. 1. Distorted five-coordinate trigonal bipyramidal active site geometry of native human MnSOD. A top view is shown as seen by approaching substrate. Sidechains of the manganese inner-sphere ligands and all residues within 7 Å of the metal are shown. The manganese is a pink sphere. Chain A is shown in yellow and chain C in magenta. Glu162 contributes to the active site from across the dimer interface. The hydrogen bond network to the manganese from bulk solvent (His30-WAT2-Tyr34-Gln143-WAT1) is indicated by dotted lines (PDB entry 5VF9). All figures were drawn using the PyMOL Molecular Graphics System, Version 1.8 Schrödinger, LLC.

Ramilo et al., 1999). Glu162 hydrogen bonds across the dimer interface to His163 from the adjacent subunit and contributes to stability and efficient catalysis (Quint et al., 2008). Both the inner and outer sphere arrangements are conserved among iron and manganese superoxide dismutases (Wintjens et al., 2004).

Two mechanisms for the activity of iron and manganese SODs have been suggested. The first is called the 5-6-5 mechanism and proposes superoxide coordinates to the active site metal and becomes molecular oxygen or hydrogen peroxide in a two-step fashion. Here the coordination state of the active site metal converts from five-coordinate trigonal bipyramidal to six-coordinate octahedral upon substrate binding and back to five-coordinate upon substrate release (Lah et al., 1995; Ludwig et al., 1991; Tierney et al., 1995). In this mechanism, anionic substrate-analogs are believed to bind in the same position as superoxide, opposite Asp159. The second mechanism observed with studies of thermochromism is called associative displacement. This mechanism proposes that six-coordinate anionic complexes represent an inactive form of the enzyme that is seen only at low temperatures. A five-coordinate complex represents the active form at physiological temperature, with anion binding displacing one of the manganese ligands, either bound water or Asp159 (Whittaker and Whittaker, 1996, 1997). The azide ion is a potent competitive inhibitor and is frequently assumed to act as a substrate analog to superoxide (Bull and Fee, 1985b; Misra and Fridovich, 1978). Published structures of azide in complex with MnSOD have been solved at room temperature for *Thermus thermophilus* (PDB entry 1MNG) and cryocooled for *Caenorhabditis elegans* (PDB entry 5AG2) (Hunter et al., 2015; Lah et al., 1995). Both show the azide binding end-on to the manganese ion at the sixth coordinate. An unpublished structure of the Y174F MnSOD-azide complex from *Escherichia coli* (PDB entry 1ZLZ) shows binding in the same manner as well, with the Y174F mutation breaking a hydrogen bond at the dimer interface. To date, the crystal structure of human MnSOD with bound azide has not been solved.

Here, the crystal structures of native human MnSOD and the human MnSOD-azide complex are reported and provide the binding position for azide in the active site. Electrostatic solvent accessible surface calculations were performed with these crystal structures to map the residues that are important for electrostatic guidance of the substrate to the active site. These surface calculations were conducted with three differing active site states, including one with superoxide coordinated using the azide binding site as a model.

2. Materials and methods

2.1. Protein purification and crystallization

Full length human MnSOD cDNA optimized for *E. coli* codons was cloned into the pACYCDuet-1 expression vector (Genscript) and transformed into the *sodA*$^{-}$*sodB*$^{-}$ strain of *E. coli*, which lacks endogenous Mn and FeSODs (Steinman, 1992). Cells were grown in Terrific Broth with 0.8% (v/v) glycerol and supplemented with 0.75 g L^{-1} $MnSO_4$ to provide the protein's active site manganese ion. Cell strain fidelity was maintained with 30 μg mL^{-1} kanamycin. Recombinant protein was expressed upon addition of 1 mM isopropyl β-D-1-thiogalactopyranoside. Cells were harvested by centrifugation and stored at -80 °C until purification. Cells were resuspended in 50 mM potassium phosphate (K_2HPO_4/KH_2PO_4), pH 7.8, prior to lysis using an Emulsiflex. Clarified lysate was incubated at 65 °C for one hour and precipitated proteins were removed by centrifugation. Soluble protein was dialyzed against 5 mM potassium phosphate, pH 7.8, and applied to pre-swollen diethylaminoethyl (DE52) cellulose resin (GE Healthcare). The protein-resin slurry was rocked for 1 h at 10 °C before vacuum filtration using Whatman #4 filter paper and a Büchner funnel. Resin was washed with an excess of 5 mM potassium phosphate, pH 7.8, then protein was eluted with 100 mM potassium phosphate, pH 7.8. Eluted protein was dialyzed against 2.5 mM 2-(N-morpholino)ethanesulfonic acid (MES), pH 5.5, applied to a carboxymethyl (CM) Sepharose (GE Healthcare) column, and eluted with a NaCl gradient. Fractions were concentrated using 5 kDa molecular weight cut-off concentrators (Sartorius) to 21 mg mL^{-1}, as measured by NanoDrop ND-1000 spectrophotometer using an extinction coefficient of 43.43 L/mol^{-1} cm^{-1} at 280 nm. Human MnSOD crystals were grown from 1.8 M potassium phosphate, pH 7.8, by hanging-drop vapor diffusion at room temperature. Protein and reservoir solution were mixed at a 1:1 ratio to give a 2.0 μL drop and crystals appeared within 1 day. To obtain the azide complex, 2.0 μL of reservoir containing 200 mM sodium azide were added to drops of 6 day crystals. Data was collected 3 h after azide addition.

2.2. Data collection and structure determination

Crystals were briefly passed through a cryoprotectant solution consisting of 3.6 M potassium phosphate, pH 7.8, using a microloop (MiTeGen). The MnSOD-azide crystals also had 150 mM sodium azide in the cryoprotectant. Crystals were plunged into a 100 K stream of nitrogen gas provided by a Rigaku X-stream. X-ray diffraction data were collected using a Rigaku FR-E Cu Kα rotating-anode generator operating at 45 kV and 45 mA equipped with a R-AXIS IV^{++} detector. Data were processed using *HKL*-3000 for indexing, integration, and scaling (Minor et al., 2006). Native MnSOD and the MnSOD-azide complex were solved using Protein Data Bank coordinates **1JA8** that had the same unit cell dimensions and space group (Hearn et al., 2001). Following removal of solvent and active-site metals, simple molecular replacement was performed through rigid-body refinement and subsequent restrained-positional refinement using *REFMAC5* to 1.82 Å and 1.77 Å resolution for the native and azide complex structures, respectively (Murshudov et al., 2011). Using *Coot*, omit electron density maps were analyzed and the protein model was fit

(Emsley and Cowtan, 2004). New solvent structure and active-site manganese ions with bound azide were modelled into omit electron density maps. Azide occupancy was determined by adjusting until the B values refined reasonably to neighboring atoms. For both native and azide structures Tyr45 of chain B was modelled with dual conformers. Geometries of the final models were verified with *MOLPROBITY* (Chen et al., 2010).

2.3. Electrostatic surface calculations

Outside the active site, pKa calculations were performed by *PROPKA 3.1* at pH 7.0 to generate partial charges. Then the partial charges were assigned on a per-atom basis in PQR file format using *PDB2PQR* within the same automated pipeline (Dolinsky et al., 2007). For the active site, partial charges from the literature (Neves et al., 2013) taking into account coordination of the manganese ion were manually applied to the PQR file. These charges also assumed a pH of 7.0. Electrostatic surfaces were generated with *APBS* using ionic strengths of 0.15 and −0.15 M for the positive and negatively charged species, respectively (Baker et al., 2001).

3. Results and discussion

X-ray diffraction data from native MnSOD and MnSOD-azide complex crystals were measured at a resolution of 1.82 Å and 1.77 Å, respectively (Table 1). Pink, hexagonal bipyramidal crystals formed in the space group $P6_122$ with unit cell dimensions of $a = b = 77.91$, $c = 237.92$ Å (native) and $a = b = 77.90$, $c = 238.44$ Å (azide complex). The crystal structures had two subunits in the asymmetric unit that were designated as chains A and B. Native oligomerization of human MnSOD consists of a tetramer formed from a dimer of dimers by crystallographic symmetry. The tetrameric interface is comprised of a four helix bundle (Borgstahl et al., 1992).

3.1. Azide binding to human MnSOD

The azide ion acts as a strong competitive inhibitor for SOD by binding directly to the active site metal (Bull and Fee, 1985b; Misra and Fridovich, 1978). The crystal structure of the human MnSOD-azide complex presented two different active sites within the crystallographic asymmetric unit. A summary of active site bond distances and angles are listed in Table 2. Chain A shows an azide molecule binding to the manganese ion at the sixth coordinate position to form a distorted octahedral active site geometry (Fig. 2a). The azide binds end-on to the metal in the position opposite Asp159 with a bond distance of 2.01 Å and an angle of 124° and widens the $N^{\varepsilon 2}$(H74)-Mn- $N^{\varepsilon 2}$(H163) angle 15° compared to the native structure. Azide also interacts with WAT2 of the hydrogen bond network, with a bond distance of 3.37 Å (Fig. 2b). The active site solvent structure is unchanged compared to the native structure for chain A, with a solvent molecule hydrogen bonded to WAT2 (designated WAT3) and another hydrogen bonded to Y34 (designated WAT4). For chain B, WAT4 of the azide soaked structure appears too far from Y34 to hydrogen bond. While the hydrogen bond network is postulated to shuttle protons to the active site for superoxide dismutation, the mechanism and protonation state of the molecules in the network are not known. For chain B, the sixth position of the active site is empty and the five-coordinate active site is the trigonal bipyramidal geometry.

The extent of azide binding to the manganese of MnSODs was measured to be no more than 50% by high field electron paramagnetic resonance spectroscopy (Tabares et al., 2006). This is in good agreement with the estimate of 40% occupancy of azide molecules found in human MnSOD electron density maps of chain A. Also, it compares well with the other published MnSOD-azide complex crystal structures, with 50% occupancy for *T. thermophilus* and 30% occupancy for *C. elegans*. The average azide B factor of 16 Å^2 illustrates a firm presence of the molecules. Azide molecules were not found elsewhere in the electron density maps.

In the three other MnSOD-azide structures, from *T. thermophilus* (PDB entry 1MNG), *C. elegans* (PDB entry 5AG2), and Y174F *E. coli* (PDB entry 1ZLZ) the azide is bound end-on at the active site manganese with the same coordination but with differing bond distances and angles (Fig. 2c). The only structure with 100%

Table 1
Crystallographic data and refinement statistics Values for the outer resolution shell are given in parentheses.

	hMnSOD	hMnSOD-azide
A. *Data collection statistics*		
Diffraction source	Rigaku FRE Cu Kα rotating-anode generator	Rigaku FRE Cu Kα rotating-anode generator
Wavelength (Å)	1.5418	1.5418
Temperature (K)	100	100
Detector	R-Axis IV++	R-Axis IV++
Crystal-detector distance (mm)	240	240
Rotation range per image (°)	0.5	0.5
Exposure time per image (s)	300	300
Space group	$P6_122$	$P6_122$
No. of molecules in asymmetric unit	2	2
$a = b$ (Å)	78.24	77.90
c (Å)	238.47	238.44
α = β (°)	90	90
γ (°)	120	120
Mosaicity (°)	0.72	0.78
Resolution range (Å)	67.5–1.82 (1.85–1.82)	67.5–1.77 (1.80–1.77)
Total No. of reflections	231836	229527
No. of unique reflections	38400	40060
Completeness (%)	96.8 (89.6)	96.0 (84.0)
Redundancy	6.0 (4.6)	5.6 (3.6)
$\langle I/\sigma(I)\rangle$	20.6 (3.0)	12.7 (2.0)
R_{meas}[a]	0.08 (0.38)	0.16 (0.59)
B. *Refinement statistics*		
PDB ID	5VF9	5T30
Resolution range (Å)	67.76–1.82	67.46–1.77
Completeness (%)	96.5	94.0
No. of reflections, working set	36515 (2434)	40053 (3139)
No. of reflections, test set	1885 (162)	1964 (148)
Final R_{cryst}	0.201	0.216
Final R_{free}	0.225	0.243
No. of Protein non-H atoms	3174	3171
Manganese ions	2	2
Phosphate ions	2	2
Potassium ions	1	2
Azide	0	1 (x 0.4)
Water	305	354
R.m.s. deviations		
Bonds (Å)	0.009	0.010
Angles (°)	1.31	1.33
Mean B factors (Å^2)		
Protein	21	20
Manganese ions	17	14
Phosphate ions	40	37
Potassium ions	23	24
Azide	–	16
Water	26	24

[a] $R_{meas} = \Sigma_{hkl}\sqrt{\frac{n}{n-1}}\Sigma_{j=1}^{n}|I_{hkl,j} - \langle I_{hkl}\rangle|/\Sigma_{hkl}\Sigma_j I_{hkl,j}$

Table 2
Active Site Geometry.

	hMnSOD		hMnSOD-azide	
	Chain A	Chain B	Chain A	Chain B
Covalent bond (Å)				
Mn-$N^{\varepsilon 2}$(H26)	2.25	2.23	2.06	2.07
Mn-$N^{\varepsilon 2}$(H74)	2.25	2.25	2.07	2.07
Mn-$O^{\delta 2}$(D159)	2.03	2.04	1.96	1.93
Mn-$N^{\varepsilon 2}$(H163)	2.25	2.25	2.05	2.06
Mn-O(WAT1)	2.17	2.15	1.94	1.95
Mn-N3(AZI)	–	–	2.01	–
Hydrogen Bonds (Å)				
$N^{\varepsilon 2}$(Q143)-O(WAT1)	2.83	2.75	3.17	3.1
$N^{\varepsilon 2}$(Q143)-OH(Y34)	2.92	2.83	2.93	2.91
O(WAT2)-OH(Y34)	2.64	2.66	2.78	2.77
O(WAT2)-$N^{\delta 1}$(H30)	2.73	2.75	2.67	2.69
O(WAT4)-OH(Y34)	2.83	3.2	2.5	4.72
O(WAT2)-O(WAT4)	2.65	2.56	2.97	4.35
O(WAT3)-O(WAT2)	2.59	2.6	2.69	2.65
O(WAT2)-N3(AZI)	–	–	3.37	–
Bond angles (°)				
$N^{\varepsilon 2}$(H26)-Mn- $N^{\varepsilon 2}$(H74)	89	91	94	93
$N^{\varepsilon 2}$(H26)-Mn-$O^{\delta 2}$(D159)	85	82	85	85
$N^{\varepsilon 2}$(H26)-Mn- $N^{\varepsilon 2}$(H163)	94	94	92	91
$N^{\varepsilon 2}$(H26)-Mn-O(WAT1)	172	172	164	167
$N^{\varepsilon 2}$(H74)-Mn-$O^{\delta 2}$(D159)	108	108	101	103
$N^{\varepsilon 2}$(H74)-Mn- $N^{\varepsilon 2}$(H163)	129	129	144	141
$N^{\varepsilon 2}$(H74)-Mn-O(WAT1)	94	90	92	94
$O^{\delta 2}$(D159)-Mn- $N^{\varepsilon 2}$(H163)	123	123	115	116
$O^{\delta 2}$(D159)-Mn-O(WAT1)	87	90	79	83
$N^{\varepsilon 2}$(H163)-Mn-O(WAT1)	89	92	92	91
$N^{\varepsilon 2}$(H26)-Mn-N3(AZI)	–	–	94	–
$N^{\varepsilon 2}$(H74)-Mn-N3(AZI)	–	–	76	–
$O^{\delta 2}$(D159)-Mn-N3(AZI)	–	–	177	–
$N^{\varepsilon 2}$(H163)-Mn-N3(AZI)	–	–	68	–
Mn-N3(AZI)-N2(AZI)	–	–	124	–
N1(AZI)-N2(AZI)-N3(AZI)	–	–	179	–

occupancy for azide is 1ZLZ with the Y174F mutation. The other structures have partial occupancies and this complicates the interpretation of the analysis as the crystal structures represent an average between 5- and 6-coordinate active sites. The prokaryotic structures show a bond distance of 2.2 Å and an angle of 143° from *T. thermophilus* and a bond distance of 1.94 Å and an angle of 123° from *E. coli*. The eukaryotic *C. elegans* structure has a bond distance of 2.8 Å and an angle of 94°. All of the azide structures widen the $N^{\varepsilon 2}$(H74)-Mn- $N^{\varepsilon 2}$(H163) angle compared to their native forms. Of note, the azide molecule in the prokaryotic *T. thermophilus* structure is orientated differently than the eukaryotic structures, with the terminal N atom furthest from the manganese replacing the position of WAT2 and the geometry of the molecule deviating slightly from linearity, with a N1-N2-N3 angle of 175°. It is also noteworthy that the *T. thermophilus* structure is the only one determined at room temperature. The *E. coli* MnSOD-azide bond distance and angle are most similar to the human structure, with a 0.7 Å difference in bonding distance and identical bonding angle.

There are other subtle structural differences in the active site solvent. WAT2 of both structures and both chains has a B value near 30 $Å^2$ compared to the average solvent values of 26 and 24 $Å^2$ of the native and azide structures, respectively. While WAT2 is the least-defined atom of the hydrogen bond network in our structures, its higher B factor may be reflective of a dynamic nature during catalysis, and the same feature has been observed in the 100 K MnSOD structure from *C. elegans* (Hunter et al., 2015). The 100 K structure from *E. coli* reveals a well-defined WAT2, with an average B value of 18 $Å^2$ between the four chains among an average solvent value of 28 $Å^2$ (Borgstahl et al., 2000). Studies of the catalytic mechanism have relied on the presence of WAT2 to shuttle protons to the active site metal but its presence in crystal structures may be a feature of cryocooling (Abreu et al., 2005).

3.2. Electrostatic guidance of anionic substrate to the active site

Due to the anionic nature of the substrate, the solvent accessible surface area near the active site was hypothesized to be basic (Getzoff et al., 1983). To study this, three electrostatic surfaces of the human MnSOD tetramer were calculated with differing active site coordination of an oxidized manganese ion (Mn^{3+}): (1) five-coordinate with water as the solvent ligand (Fig. 3a), (2) five-coordinate with hydroxide as the solvent ligand (Fig. 3b), and (3) six-coordinate with hydroxide and superoxide ligands (Fig. 3c). The position of the superoxide was modelled from the first two nitrogen atoms of the azide bound to the active site manganese in chain A. For these calculations, the partial charges for the atoms of all molecules ligated to the manganese ion were obtained from the work of Neves and coworkers (Neves et al., 2013). These complexes represent the first half of the dismutation reaction. Unfortunately, partial charges for reduced manganese (Mn^{2+}) are currently not available.

The resulting electrostatic surfaces reveal how substrate diffusion to the active site could be enhanced. Of the three coordination states modelled, the electrostatic surface near the five coordinate active site "pit", with water as the solvent ligand, is the most basic (Fig. 3d). The pit is also more basic than the rest of the tetramer and there is a "valley" of positively-charged patches surrounding the pit (Fig. 3g). Coordination of hydroxide as the solvent ligand instead of water lowers the electrostatic surface potential of the active site pit (Fig. 3e). The differing active site states had no effect on the electrostatic surface potentials of the valleys (Fig. 3h,i). The

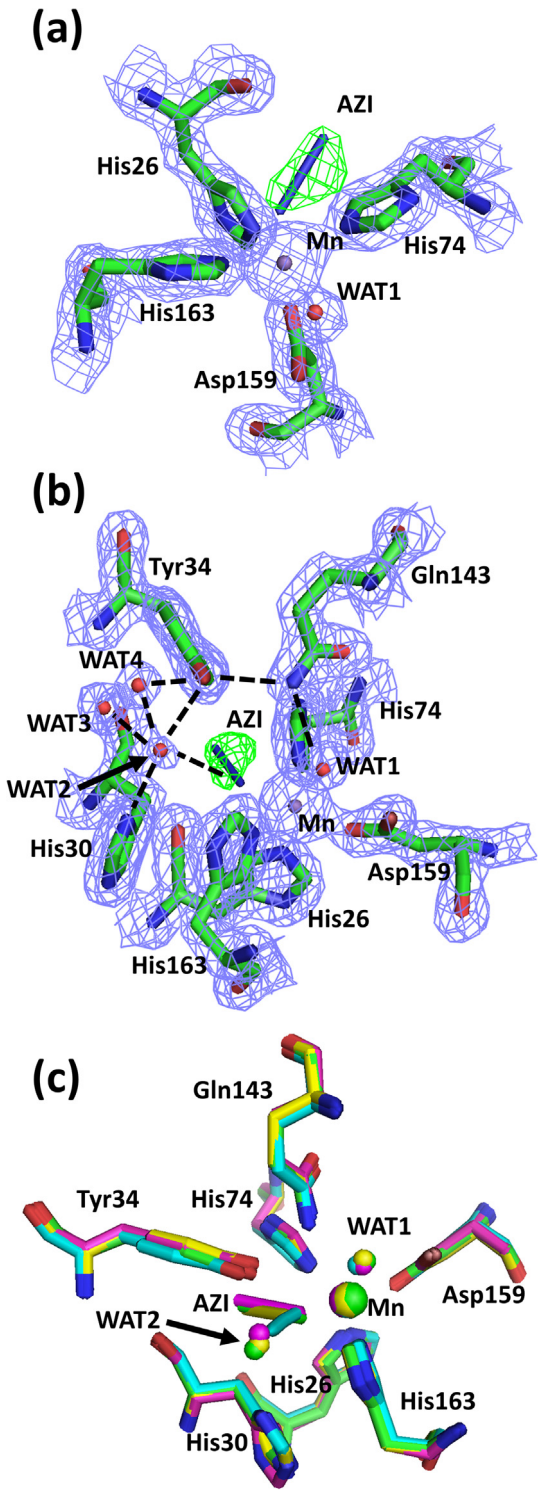

Fig. 2. Active site geometry and electron density of azide-soaked human MnSOD. Black, dashed lines indicate hydrogen bonds. (a) Six coordinate octahedral active site geometry at chain A. (b) Azide interaction with the active site hydrogen bond network at chain A. Maps were calculated before azide was modelled and refined with Fourier coefficients Fo–Fc (green) contoured at 3.0σ, and 2Fo–Fc density (blue) contoured at 1.5 σ. (c) Active site overlays of MnSOD-azide complexes from *T. thermophilus* (cyan, PDB entry **1MNG**), *C. elegans* (yellow, PDB entry 5AG2), *E. coli* (pink, PDB entry 1ZLZ) and human (green, PDB entry 5T30). Overlays were performed using *SUPERPOSE* (Krissinel and Henrick, 2004).

six coordinate active site pit with superoxide bound with hydroxide as the solvent ligand has a nearly neutral electrostatic surface potential at the pit (Fig. 3f). Azide and hydroxide are known inhibitors of SODs and bind to the sixth coordinate position, presumably like superoxide (Borgstahl et al., 2000; Lah et al., 1995; Ludwig et al., 1991; Tierney et al., 1995). Binding of these inhibitors to the active site could neutralize the surface potential like superoxide does and provide yet another means of inhibition.

Direct evidence on whether the coordinated solvent ligand is a water molecule (Mn^{3+}-OH_2, Fig. 3a) or a hydroxide molecule (Mn^{3+}-OH^-, Fig. 3b) has been difficult to discern due to experimental limitations. Steady-state kinetic analysis of FeSOD from *E. coli* suggest the oxidized iron has a hydroxide ligand coordinated (Fe^{3+}-OH^-) and proton uptake at the active site upon reduction of the metal ion results in Fe^{2+}-OH_2 (Bull and Fee, 1985a). NMR studies of FeSOD and MnSOD from *E. coli* reveal that amino acids at the active site do not become protonated upon metal ion reduction and the solvent ligand is the most probable proton accepter (Miller et al., 2003). Further studies using density function calculations show that such protonation is energetically favourable in both *E. coli* FeSOD and human MnSOD (Abreu et al., 2005). These studies support the Mn^{3+}-OH^- state as the most chemically likely.

3.3. Players in electrostatic guidance and substrate entry into the active site

The most influential residues to the electrostatic surface potential were identified by mapping charged residues to the surface (Fig. 4a). The outer ridge is populated by negatively-charged glutamate and aspartate residues while positively-charged lysine and arginine residues are found in the active site valley and pit. The residues from both subunits at the dimeric interface (red dashed line, Fig. 4a) combine to form a valley of positive surface potential. These calculations indicate that anionic substrate is repelled away from the negatively-charged outer ridge of the human MnSOD tetramer and attracted into the center, towards an active site.

A cross-section view of the active site pit provides insight into the interaction of superoxide with the surface that enhances collision with the metal ion (Fig. 4b). Three positively-charged residues contribute to the basic surface potential at the active site pit, Lys29 of chain A and Arg173 and Lys178 of chain C. For *E. coli* MnSOD, an electrostatic surface study also found a positively charged active site pit with a similar cluster of positively charged residues, consisting of four arginine residues contributed by two chains (Edwards et al., 2001a).

The high rate constant of MnSOD indicates that nearly all collisions to the active site are productive, and electrostatic forces may provide some pre-collision orientation. The placement of Glu162 and Arg173 6 Å apart may contribute to the effective diffusion of substrate into the active site. Glu162 is the closest negatively charged residue to the manganese ion, being 7 Å away, and Arg173 is the closest positively charged residue, being 12 Å away. Arg173 could draw in anionic substrate toward the gateway residues while Glu162 prevents non-productive association with Arg173. A similar pair of amino acids have been suggested for bovine CuZnSOD, where Glu131 and Lys134 were found to work together to diffuse superoxide towards the active site (Getzoff et al., 1983).

Glu162 and Arg173 are conserved spatially in the *C. elegans*, *T. thermophilus*, and *E. coli* MnSOD structures (PDB entries **5AG2, 1MNG,** and **1D5N**, respectively) and appear to be important for catalytic activity. Glu162 from across the dimer interface hydrogen bonds with Mn ligand His163. In *E. coli* MnSOD, residue Glu170 (Glu162 in human) is essential for dimer stability and metal selectivity (Whittaker and Whittaker, 1998). For human MnSOD, Glu162Asp and Glu162Ala mutations retain the tetramer but activity is decreased 5–25% and the level of product inhibition is increased 2-fold (Quint et al., 2008), indicating that Glu162 fulfils

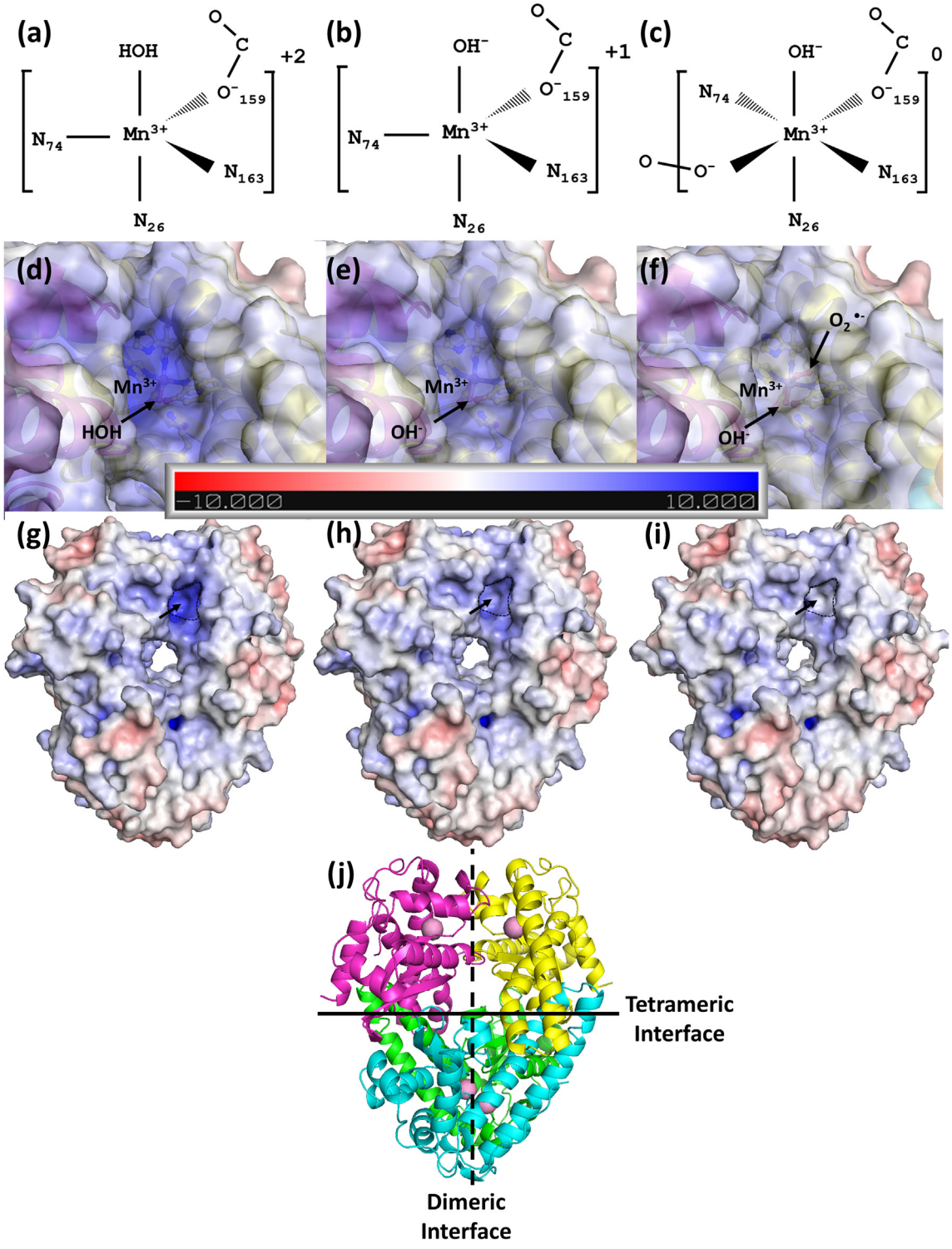

Fig. 3. Solvent accessible (sphere radius = 1.4 Å) electrostatic surfaces of oxidized human MnSOD with differing active site coordination. (a–c) Differing models of active site coordination used to generate the subsequent electrostatic surfaces. (d–f) Electrostatic potential at the active site quantified in kT. (g–i) Electrostatic potential of the tetramer. Arrow indicates one of four active sites seen with this orientation. (j) Ribbon diagram of the tetramer. Pink spheres indicate manganese ions and location of the active sites. Vertical dashed line indicates the dimeric interface that is evolutionarily conserved and the horizontal line indicates the tetrameric interface.

more than an electrostatic role. Previous studies have shown a positive charge at position 173 is essential for catalysis and enzyme activity can be abolished by chemical modification at this site (Borders et al., 1991; Chan et al., 1990) This model of human MnSOD indicates that positively-charged residues line the active site pit and strategic placement of Glu162 and Arg173 may contribute to productive interaction of anionic substrate with the active site.

Human MnSOD activity is regulated by post translational modifications (Ozden et al., 2011; Sarsour et al., 2014). The activity of MnSOD in cells is reduced through acetylation of lysines (Qiu et al., 2010; Tao et al., 2010). Acetylation causes lysines to

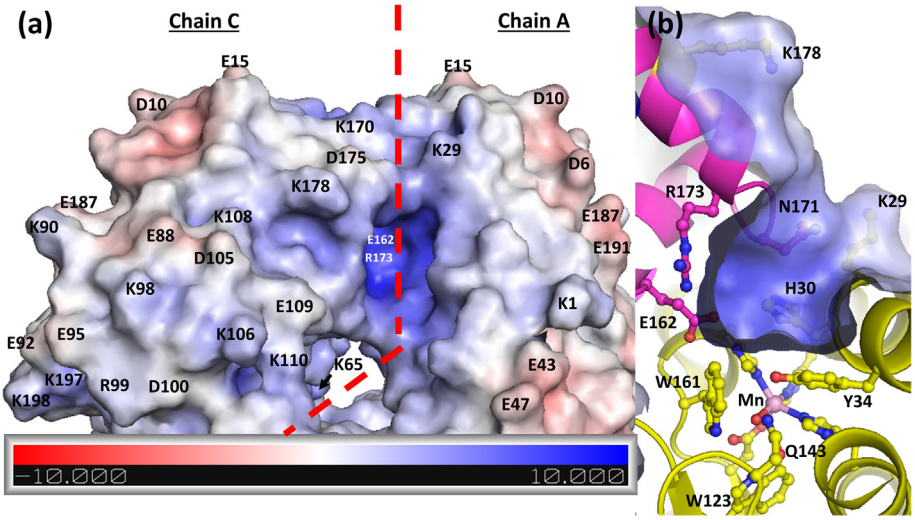

Fig. 4. Charged surface residues that contribute to the electrostatic surface potential of human MnSOD in the Mn^{3+}-OH_2 state. (a) Charged residues of chains A and C found to contribute to the solvent accessible surface area by *AREAIMOL* (Collaborative Computational Project, 1994) were mapped. The red, dashed line indicates the dimeric interface and thus the boundary separating the chains. The label for Glu162 and Arg173 is white to indicate their location on the concave surface within the active site pit. (b) The active site pit formed by the dimeric interface. Glu162 is behind Arg173 in this view. Chain A is yellow and chain C is magenta. This side view of the active site pit is rotated approximately 90° relative to Fig. 1.

be neutral in charge and presumably decreases superoxide attraction to the active site. Changes in net charge of the protein via acetylated lysines, even if far from the active site, could change the vector direction of the electrostatic field, as exemplified by Getzoff and coworkers (Getzoff et al., 1983). Also, mass spectrometric analysis showed that Arg173 is dimethylated in proliferating and quiescent human fibroblast cells (Sarsour et al., 2012). Methylation does not change the net charge of the arginine residue but adds bulky groups and reorients the charge. The functional role of Arg173 methylation and contribution to activity is unclear. How posttranslational modifications regulate MnSOD activity are of medical interest and the topic of future mechanistic studies.

4. Conclusions

The crystal structure of the human MnSOD-azide complex, and in conjunction with electrostatic surface calculations, provides a model for the entry and binding position of the superoxide substrate to the active site. When inferring mechanistic data from the postulated superoxide binding site, the human and the recent *C. elegans* structures provide better models when comparing eukaryotic MnSOD structures. Electrostatic calculations suggest anionic substrate is guided toward the active site of MnSOD by a negatively-charged outer ridge and positively charged central valleys. Superoxide is then correctly oriented by Glu162 and Arg173, enters the active site by passing residues Tyr34 and His30, and binds to the manganese ion at the sixth coordinate position.

Accession numbers

Atomic coordinates and structure factors have been deposited in the Protein Data Bank with accession codes **5VF9** (native human MnSOD) and **5T30** (human MnSOD-azide complex).

Conflict of interest

The authors declare no competing financial interests.

Acknowledgements

We would like to thank Anne-Francis Miller (University of Kentucky) for generously providing the *sodA*$^{-}$*sodB*$^{-}$ strain of *E. coli*. We thank Carol Kolar and Jeffrey Lovelace for useful discussions and technical assistance. This research was supported by NASA EPSCoR funding (44-0307-1021-201). The UNMC Structural Biology CORE Facility was funded by the following National Institutes of Health (NIH) grants: the Fred & Pamela Buffett Cancer Center Support Grant (P30CA036727), National Center for Research Resources grant 5P20RR016469, and the National Institute for General Medical Science grant 8P20GM103427.

Appendix A. Supplementary data

Supplementary data associated with this article can be found, in the online version, at http://dx.doi.org/10.1016/j.jsb.2017.04.011.

References

Abreu, I.A., Rodriguez, J.A., Cabelli, D.E., 2005. Theoretical studies of manganese and iron superoxide dismutases: superoxide binding and superoxide oxidation. J. Phys. Chem. B 109, 24502–24509.
Baker, N.A., Sept, D., Joseph, S., Holst, M.J., McCammon, J.A., 2001. Electrostatics of nanosystems: application to microtubules and the ribosome. Proc. Natl. Acad. Sci. U. S. A. 98, 10037–10041.
Bannister, W.H., Bannister, J.V., 1987. Factor analysis of the activities of superoxide dismutase, catalase and glutathione peroxidase in normal tissues and neoplastic cell lines. Free Radic. Res. Commun. 4, 1–13.
Borders Jr., C.L., Chain, V.W., Bjerrum, M.J., 1991. The positive charge at position 189 is essential for the catalytic activity of iron- and manganese-containing superoxide dismutases. Free Radic. Res. Commun. 12–13 (Pt 1), 279–285.
Borgstahl, G.E., Parge, H.E., Hickey, M.J., Beyer Jr., W.F., Hallewell, R.A., Tainer, J.A., 1992. The structure of human mitochondrial manganese superoxide dismutase reveals a novel tetrameric interface of two 4-helix bundles. Cell 71, 107–118.
Borgstahl, G.E., Pokross, M., Chehab, R., Sekher, A., Snell, E.H., 2000. Cryo-trapping the six-coordinate, distorted-octahedral active site of manganese superoxide dismutase. J. Mol. Biol. 296, 951–959.
Bull, C., Fee, J.A., 1985a. Steady-state kinetic studies of superoxide dismutases: properties of the iron containing protein from Escherichia coli. J. Am. Chem. Soc. 107, 3295–3304.
Bull, C., Fee, J.A., 1985b. Steady-State Kinetic Studies of Superoxide Dismutases: Properties of the Iron Containing Protein from *Escherichia coli*. J. Am. Chem. Soc. 107, 3295–3304.
Chan, V.W., Bjerrum, M.J., Borders Jr., C.L., 1990. Evidence that chemical modification of a positively charged residue at position 189 causes the loss of

catalytic activity of iron-containing and manganese-containing superoxide dismutases. Arch. Biochem. Biophys. 279, 195–201.
Chen, V.B., Arendall 3rd, W.B., Headd, J.J., Keedy, D.A., Immormino, R.M., Kapral, G.J., Murray, L.W., Richardson, J.S., Richardson, D.C., 2010. MolProbity: all-atom structure validation for macromolecular crystallography. Acta Crystallogr. D Biol. Crystallogr. 66, 12–21.
Collaborative Computational Project, Number 4, 1994. The CCP4 suite: programs for protein crystallography. Acta crystallogr. Sect. D 50, 760–763.
Dolinsky, T.J., Czodrowski, P., Li, H., Nielsen, J.E., Jensen, J.H., Klebe, G., Baker, N.A., 2007. PDB2PQR: expanding and upgrading automated preparation of biomolecular structures for molecular simulations. Nucleic Acids Res. 35, W522–W525.
Edwards, R.A., Whittaker, M.M., Whittaker, J.W., Baker, E.N., Jameson, G.B., 2001a. Removing a hydrogen bond in the dimer interface of Escherichia coli manganese superoxide dismutase alters structure and reactivity. Biochemistry 40, 4622–4632.
Edwards, R.A., Whittaker, M.M., Whittaker, J.W., Baker, E.N., Jameson, G.B., 2001b. Outer sphere mutations perturb metal reactivity in manganese superoxide dismutase. Biochemistry 40, 15–27.
Emsley, P., Cowtan, K., 2004. Coot: model-building tools for molecular graphics. Acta Crystallogr. D 60, 2126–2132.
Getzoff, E.D., Tainer, J.A., Weiner, P.K., Kollman, P.A., Richardson, J.S., Richardson, D. C., 1983. Electrostatic recognition between superoxide and copper, zinc superoxide dismutase. Nature 306, 287–290.
Hearn, A.S., Stroupe, M.E., Cabelli, D.E., Lepock, J.R., Tainer, J.A., Nick, H.S., Silverman, D.N., 2001. Kinetic analysis of product inhibition in human manganese superoxide dismutase. Biochemistry 40, 12051–12058.
Holm, R.H., Kennepohl, P., Solomon, E.I., 1996. Structural and functional aspects of metal sites in biology. Chem. Rev. 96, 2239–2314.
Hunter, G.J., Trinh, C.H., Bonetta, R., Stewart, E.E., Cabelli, D.E., Hunter, T., 2015. The structure of the Caenorhabditis elegans manganese superoxide dismutase MnSOD-3-azide complex. Protein Sci. 24, 1777–1788.
Kim, A., 2010. Modulation of MnSOD in cancer: epidemiological and experimental evidence. Toxicol. Res. 26, 83–93.
Krissinel, E., Henrick, K., 2004. Secondary-structure matching (SSM), a new tool for fast protein structure alignment in three dimensions. Acta Crystallogr. D 60, 2256–2268.
Lah, M.S., Dixon, M.M., Pattridge, K.A., Stallings, W.C., Fee, J.A., Ludwig, M.L., 1995. Structure-function in Escherichia coli iron superoxide dismutase: comparisons with the manganese enzyme from Thermus thermophilus. Biochemistry 34, 1646–1660.
Leveque, V.J., Stroupe, M.E., Lepock, J.R., Cabelli, D.E., Tainer, J.A., Nick, H.S., Silverman, D.N., 2000. Multiple replacements of glutamine 143 in human manganese superoxide dismutase: effects on structure, stability, and catalysis. Biochemistry 39, 7131–7137.
Li, Y., Huang, T.T., Carlson, E.J., Melov, S., Ursell, P.C., Olson, J.L., Noble, L.J., Yoshimura, M.P., Berger, C., Chan, P.H., Wallace, D.C., Epstein, C.J., 1995. Dilated cardiomyopathy and neonatal lethality in mutant mice lacking manganese superoxide dismutase. Nat. Genet. 11, 376–381.
Ludwig, M.L., Metzger, A.L., Pattridge, K.A., Stallings, W.C., 1991. Manganese superoxide dismutase from Thermus thermophilus. A structural model refined at 1.8 A resolution. J. Mol. Biol. 219, 335–358.
McCord, J.M., 2002. Superoxide dismutase in aging and disease: an overview. Methods Enzymol. 349, 331–341.
Miller, A.F., Padmakumar, K., Sorkin, D.L., Karapetian, A., Vance, C.K., 2003. Proton-coupled electron transfer in Fe-superoxide dismutase and Mn-superoxide dismutase. J. Inorg. Biochem. 93, 71–83.
Minor, W., Cymborowski, M., Otwinowski, Z., Chruszcz, M., 2006. HKL-3000: the integration of data reduction and structure solution–from diffraction images to an initial model in minutes. Acta Crystallogr. D Biol. Crystallogr. 62, 859–866.
Misra, H.P., Fridovich, I., 1978. Inhibition of superoxide dismutases by azide. Arch. Biochem. Biophys. 189, 317–322.
Murshudov, G.N., Skubak, P., Lebedev, A.A., Pannu, N.S., Steiner, R.A., Nicholls, R.A., Winn, M.D., Long, F., Vagin, A.A., 2011. REFMAC5 for the refinement of macromolecular crystal structures. Acta Crystallogr. D 67, 355–367.
Neves, R.P., Sousa, S.F., Fernandes, P.A., Ramos, M.J., 2013. Parameters for molecular dynamics simulations of manganese-containing metalloproteins. J. Chem. Theory Comput. 9, 2718–2732.
Ozden, O., Park, S.H., Kim, H.S., Jiang, H., Coleman, M.C., Spitz, D.R., Gius, D., 2011. Acetylation of MnSOD directs enzymatic activity responding to cellular nutrient status or oxidative stress. Aging (Albany NY) 3, 102–107.
Perry, J.J., Fan, L., Tainer, J.A., 2007. Developing master keys to brain pathology, cancer and aging from the structural biology of proteins controlling reactive oxygen species and DNA repair. Neuroscience 145, 1280–1299.
Perry, J.J., Hearn, A.S., Cabelli, D.E., Nick, H.S., Tainer, J.A., Silverman, D.N., 2009. Contribution of human manganese superoxide dismutase tyrosine 34 to structure and catalysis. Biochemistry 48, 3417–3424.
Qiu, X., Brown, K., Hirschey, M.D., Verdin, E., Chen, D., 2010. Calorie restriction reduces oxidative stress by SIRT3-mediated SOD2 activation. Cell Metab. 12, 662–667.
Quint, P.S., Domsic, J.F., Cabelli, D.E., McKenna, R., Silverman, D.N., 2008. Role of a glutamate bridge spanning the dimeric interface of human manganese superoxide dismutase. Biochemistry 47, 4621–4628.
Ramilo, C.A., Leveque, V., Guan, Y., Lepock, J.R., Tainer, J.A., Nick, H.S., Silverman, D. N., 1999. Interrupting the hydrogen bond network at the active site of human manganese superoxide dismutase. J. Biol. Chem. 274, 27711–27716.
Sarsour, E.H., Kalen, A.L., Xiao, Z., Veenstra, T.D., Chaudhuri, L., Venkataraman, S., Reigan, P., Buettner, G.R., Goswami, P.C., 2012. Manganese superoxide dismutase regulates a metabolic switch during the mammalian cell cycle. Cancer Res. 72, 3807–3816.
Sarsour, E.H., Kalen, A.L., Goswami, P.C., 2014. Manganese superoxide dismutase regulates a redox cycle within the cell cycle. Antioxid. Redox Signal. 20, 1618–1627.
Steinman, H.M., 1992. Construction of an Escherichia coli K-12 strain deleted for manganese and iron superoxide dismutase genes and its use in cloning the iron superoxide dismutase gene of Legionella pneumophila. Mol. Gen. Genet. 232, 427–430.
Sun, J., Folk, D., Bradley, T.J., Tower, J., 2002. Induced overexpression of mitochondrial Mn-superoxide dismutase extends the life span of adult Drosophila melanogaster. Genetics 161, 661–672.
Tabares, L.C., Cortez, N., Hiraoka, B.Y., Yamakura, F., Un, S., 2006. Effects of substrate analogues and pH on manganese superoxide dismutases. Biochemistry 45, 1919–1929.
Tao, R., Coleman, M.C., Pennington, J.D., Ozden, O., Park, S.H., Jiang, H., Kim, H.S., Flynn, C.R., Hill, S., Hayes McDonald, W., Olivier, A.K., Spitz, D.R., Gius, D., 2010. Sirt3-mediated deacetylation of evolutionarily conserved lysine 122 regulates MnSOD activity in response to stress. Mol. Cell 40, 893–904.
Tierney, D.L., Fee, J.A., Ludwig, M.L., Penner-Hahn, J.E., 1995. X-ray absorption spectroscopy of the iron site in Escherichia coli Fe(III) superoxide dismutase. Biochemistry 34, 1661–1668.
Whittaker, M.M., Whittaker, J.W., 1996. Low-temperature thermochromism marks a change in coordination for the metal ion in manganese superoxide dismutase. Biochemistry 35, 6762–6770.
Whittaker, M.M., Whittaker, J.W., 1997. A "thermophilic shift" in ligand interactions for thurmus thermophilus manganese superoxide dismutase. J. Biol. Inorg. Chem. 2, 667–671.
Whittaker, M.M., Whittaker, J.W., 1998. A glutamate bridge is essential for dimer stability and metal selectivity in manganese superoxide dismutase. J. Biol. Chem. 273, 22188–22193.
Wintjens, R., Noel, C., May, A.C., Gerbod, D., Dufernez, F., Capron, M., Viscogliosi, E., Rooman, M., 2004. Specificity and phenetic relationships of iron- and manganese-containing superoxide dismutases on the basis of structure and sequence comparisons. J. Biol. Chem. 279, 9248–9254.